Propulsion of African trypanosomes is driven by bihelical waves with alternating chirality separated by kinks

Jose A. Rodríguez[a,b], Miguel A. Lopez[c], Michelle C. Thayer[c], Yunzhe Zhao[d], Michael Oberholzer[c], Donald D. Chang[d], Neville K. Kisalu[c], Manuel L. Penichet[a,b,c], Gustavo Helguera[b], Robijn Bruinsma[d], Kent L. Hill[a,c], and Jianwei Miao[d,1]

[a]Molecular Biology Institute, [b]Department of Surgery, Division of Surgical Oncology, and [c]Department of Microbiology Immunology and Molecular Genetics, The David Geffen School of Medicine, and [d]Department of Physics and Astronomy, University of California, Los Angeles, CA 90095

Edited by Howard C. Berg, Harvard University, Cambridge, MA, and approved September 16, 2009 (received for review June 23, 2009)

***Trypanosoma brucei*, a parasitic protist with a single flagellum, is the causative agent of African sleeping sickness. Propulsion of *T. brucei* was long believed to be by a drill-like, helical motion. Using millisecond differential interference-contrast microscopy and analyzing image sequences of cultured procyclic-form and bloodstream-form parasites, as well as bloodstream-form cells in infected mouse blood, we find that, instead, motility of *T. brucei* is by the propagation of kinks, separating left-handed and right-handed helical waves. Kink-driven motility, previously encountered in prokaryotes, permits *T. brucei* a helical propagation mechanism while avoiding the large viscous drag associated with a net rotation of the broad end of its tapering body. Our study demonstrates that millisecond differential interference-contrast microscopy can be a useful tool for uncovering important short-time features of microorganism locomotion.**

millisecond differential interference-contrast microscopy | *Trypanosoma brucei* | cilium | flagellum

The protozoan parasite *Trypanosoma brucei* is the causative pathogen of African sleeping sickness, a fatal disease indigenous to subSaharan Africa where 60 million people are at risk of infection (1, 2). *T. brucei* is transmitted between human hosts by a tsetse fly vector, and parasite motility is important in both hosts. In the tsetse fly, procyclic-form (PCF) parasites colonize the midgut and then migrate through the alimentary canal to the salivary glands, where maturation into human infectious forms occurs (3, 4). From the salivary gland, mature parasites can be injected into the blood of a mammalian host that has been bitten by the fly. In the mammalian host, migration of bloodstream-form (BSF) parasites through the blood-brain barrier initiates onset of the fatal course of the disease (5, 6). *T. brucei* is extracellular at all stages of infection and depends on its own flagellum-mediated motility for dissemination. Flagellar motility of *T. brucei* in various environments is believed to be central not only to host-parasite interaction, but also to cell division, morphogenesis, and development (3, 6–15).

The *T. brucei* cell body is roughly 20-μm long, with a relatively large posterior section tapering off into a long, narrow anterior section. It has a single flagellum, with the classic "9 + 2" microtubule axoneme architecture that is attached to the cell body along its length. Based on microscopy studies, it is believed that propulsion of *T. brucei* proceeds by left-hand (LH) helical waves propagating along the flagellum, from tip to base, driving the cell forward in a drill-like motion (see Fig. 1*A*) (15–17). The genus name of the parasite actually derives from this distinctive motility (from the Greek *trypanon* or auger, and *soma* or body), first described in 1843 (18). Here, we use millisecond resolution differential interference-contrast (DIC) microscopy, combined with other microscopy methods, to provide a quantitative analysis of *T. brucei* cell propulsion. Our results reveal that *T. brucei* forward motility is characterized by the propagation of kinks separating helical waves of alternate chirality.

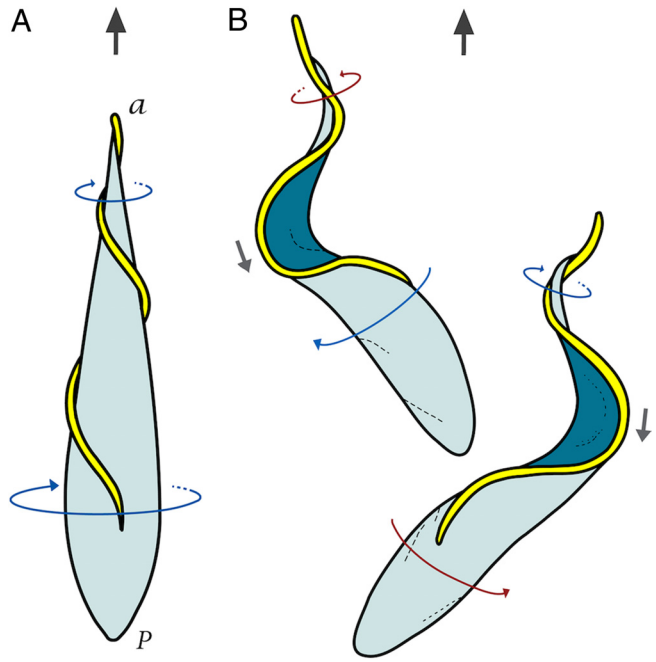

Fig. 1. Models of forward motility for *T. brucei* in aqueous media. (*A*) The traditional model: propulsion is caused by helical waves propagating from the tip to the base of the flagellum with LH chirality, resulting in a drill-like motion of the cell body (''*a*'' and ''*p*'' represent the anterior and posterior end of the cell). (*B*) The bihelical model in which alternating LH and right hand (RH) helical waves propagate down the flagellum separated by a kink. The flagellum of the bottom cell exhibits a LH helical wave (*blue arrow*) at the tip and a RH helical wave (*red arrow*) near the base, separated by a ''minus'' kink (*gray arrow*). The flagellum of the top cell shows a RH helical wave at the tip and a LH helical wave near the base, separated by a ''plus'' kink. Kinks propagate in a direction opposite to that of cell propulsion. Two dominant cell-body configurations are associated with the propagation of kinks, with the cell body rocking back and forth between the two alternating configurations.

Results

Helical Waves with Alternating Chirality. To investigate *T. brucei* propulsion in standard culture conditions, we used high-speed

Author contributions: J.A.R., R.B., K.L.H., and J.M. designed research; J.A.R., M.A.L., M.C.T., Y.Z., M.O., D.D.C., N.K.K., and J.M. performed research; J.A.R., M.A.L., M.C.T., Y.Z., M.O., D.D.C., M.L.P., G.H., R.B., K.L.H., and J.M. analyzed data; and J.A.R., R.B., K.L.H., and J.M. wrote the paper.

The authors declare no conflict of interest.

This article is a PNAS Direct Submission.

[1]To whom correspondence should be addressed. Email: miao@physics.ucla.edu.

This article contains supporting information online at www.pnas.org/cgi/content/full/0907001106/DCSupplemental.

www.pnas.org/cgi/doi/10.1073/pnas.0907001106

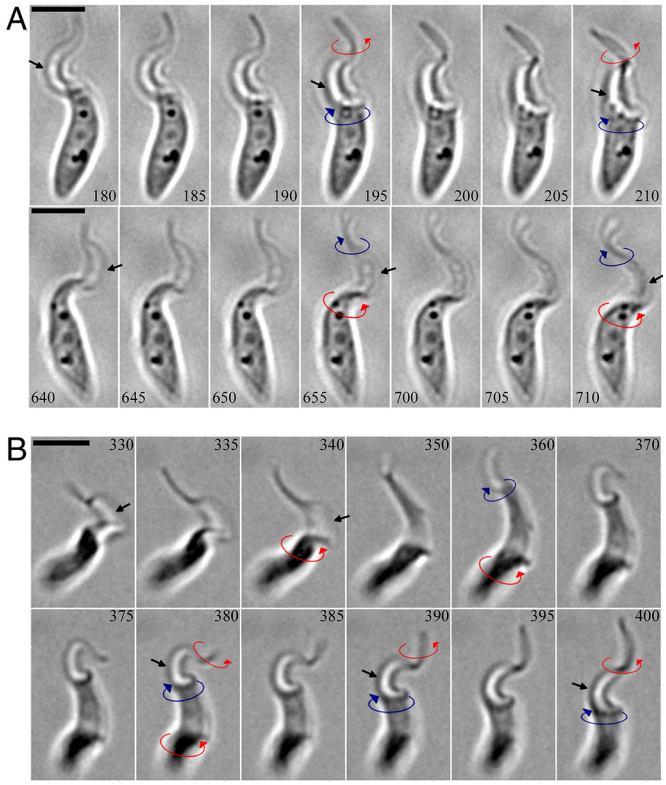

Fig. 2. Millisecond DIC microscopy imaging of PCF and BSF cell motility. (*A*) (*Top*) Image sequence of a PCF cell showing a RH (*red arrow*) helical wave at the tip and a LH (*blue arrow*) helical wave near the base of the flagellum, separated by a plus kink (*black arrow*). (*Bottom*) Image sequence of the same cell showing a LH helical wave at the tip and a RH helical wave near the base separated by a minus kink. The numerical values are in milliseconds. (Scale bars, 5 μm.) (*B*) Image sequence of a BSF cell showing bihelical waves that are separated by a minus kink (*Top*) immediately followed by a plus kink (*Bottom*).

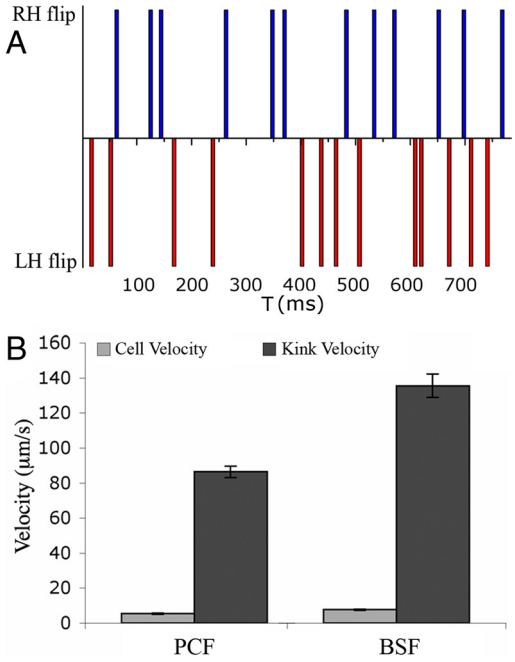

Fig. 3. Analysis of cell propulsion in PCF and BSF *T. brucei*. (*A*) Representative plot showing the distribution of the LH and RH helical waves at the anterior end of a PCF cell within a time interval of about 800 ms. The number of waves was determined by monitoring how many times the flagellum flipped to initiate a RH or LH wave, as indicated with blue and red vertical bars, respectively. Each flip represents a rotation of ≈180°. No more than three successive flips in the same direction are generated at the anterior end. Note that the rotation frequency in this example is somewhat higher than the average frequency of 19 ± 3 flips per second. (*B*) Cell velocities were calculated from 50 PCF (5 ± 2 μm/s) and 50 BSF (8 ± 2 μm/s) cells undergoing directional motion. The kink velocities were obtained from 27 kinks in five PCF cells (86 ± 3 μm/s) and 24 kinks in eight BSF cells (136 ± 7 μm/s), respectively. The ratio of the kink velocity to the cell velocity is about 16 for PCF and 18 for BSF cells.

DIC microscopy with a millisecond timescale [supporting information (SI) Fig. S1] (see *SI Text* for details]. The millisecond frame-by-frame analysis revealed that cell propulsion of *T. brucei* is characterized by repeated reversals in the rotation direction of the flagellum tip, which produced helical waves of alternating chirality propagating tip to base (Figs. 1*B* and Fig. S2, Movies S1 and S2). The image sequence in Fig. 2*A* (*Top*) shows such a bihelical wave in a PCF cell having RH chirality at the tip and LH chirality near the base of the flagellum (see Movie S1). At a later time, this same cell initiated a beat with opposite chirality (see Fig. 2*A Bottom*): that is, exhibiting LH chirality at the tip and RH chirality near the base of the flagellum. We quantified the frequency of LH and RH helical waves by tabulating how many times the flagellum tip flipped to initiate a wave in either direction. The average frequency, calculated from five cells, was 19 ± 3 flips per second, with each flip representing a rotation of ≈180°. This was split approximately equally between LH (9.7 ± 1.3 flips/s) and RH waves (9.0 ± 2.0 flips/s), as illustrated by the representative example shown in Fig. 3*A*. Typically, no more than three successive waves with the same chirality are generated at the flagellar tip. Thus, there appears to be no systematic bias for LH or RH chirality in the motility dynamics.

Next, we examined BSF *T. brucei* cells to determine whether helical waves with alternating chirality are a shared feature of both life-cycle stages. The millisecond DIC images clearly demonstrate bihelical waves in the flagellum of BSF cells (Movies S3 and S4). The image sequence in Fig. 2*B* shows a BSF cell monitored over a 70-ms time period. The top panels show a bihelical wave with LH chirality at the tip and RH chirality near the base of the flagellum. As this wave propagates toward the flagellum base, a new RH helical turn is initiated at the flagellum tip, producing a wave with RH, LH, RH chirality from tip to base (*Bottom*).

Kinks. A segment of a filament connecting two helical segments of opposite chirality is known as a "kink." We define a "plus" kink as one separating an anterior RH helical wave from a posterior LH helical wave, while a "minus" kink separates an anterior LH helical wave from a posterior RH helical wave. A kink separating two traveling helical waves, as in Fig. 2*A*, will itself travel along the filament. Traveling kinks have been encountered earlier in motility studies of prokaryotes, such as *Escherichia coli* (19, 20), where they appear to be associated with changes in course. In *Spiroplasma*, which do not have flagella (21), pairs of kinks traveling along the helical cell body cause the cell to swim in a zig-zag path. A theoretical study of *Spiroplasma* motility (22) proposed that recoil against the motion of fluid carried backwards by traveling kinks actually is the propulsive mechanism of *Spiroplasma*.

Well-defined kinks could be observed in the millisecond DIC images of both PCF and BSF *T. brucei* cells (see the *gray arrow* in Fig. 1*B*, Fig. 2, and Movies S1–S4). The kinks propagated down the flagellum along the cell body from tip to base (see Fig. 2, and Movies S1–S4), opposite to the direction of cell propulsion. Typical kink propagation velocities in *T. brucei* were 85 ± 18 μm/s in PCF cells and 136 ± 7 μm/s in BSF cells, more than an order of magnitude higher than the center-of-mass velocity of the cells (Fig. 3*B* and details in the *SI Text*). The observation that a 1.6-fold increase of kink velocity in BSF cells versus PCF cells correlates with a 1.6-fold increase in the center-of-mass velocity of BSF versus

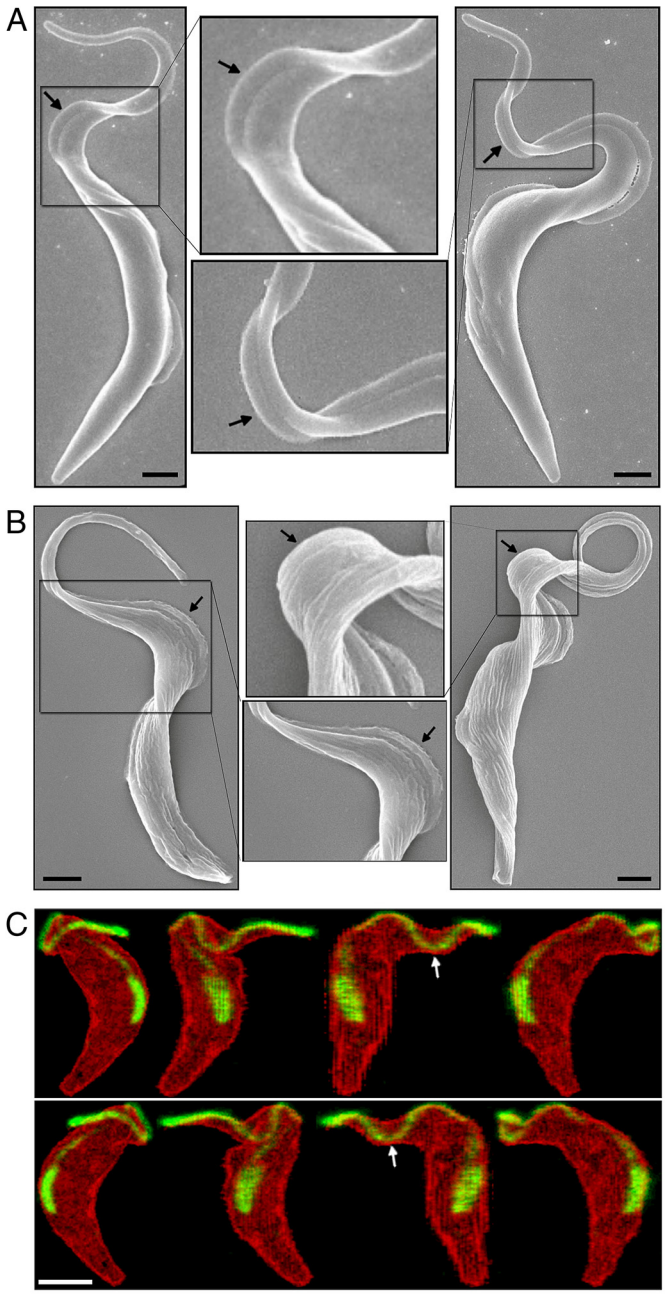

Fig. 4. SEM and confocal microscopy imaging of rapid-fixed PCF and BSF cells. (*A*) SEM images of PCF cells with bihelical waves separated by a plus (*Left*) or a minus (*Right*) kink. (*B*) SEM images of BSF cells with bihelical waves separated by a plus (*Left*) or a minus (*Right*) kink. The zoom-in views illustrate torsion of the cell body induced by the bihelical waves and kinks. (Scale bars, 1 μm.) (*C*) Confocal microscopy images of a GFP-labeled flagellum in a single PCF cell (see Movie S5). The cell is rotated along the vertical axis with $\approx$45° per image. The flagellum (*green*) wrapping around the surface of the cell body (*red*) exhibits RH chirality near the base and LH chirality near the tip, forming a minus kink (*white arrows*). (Scale bar, 3 μm.)

PCF cells (see Fig. 3*B*) suggests that kink motion is intrinsic to the propagation mechanism.

To further confirm the existence of helical waves and kinks in *T. brucei*, we used scanning electron microscopy (SEM) combined with a rapid-fixation technique that was optimized to preserve flagellar waveforms (23). SEM images of rapid-fixed cells indeed revealed bihelical waves and kinks in both PCF and BSF cells (Fig. 4 *A* and *B*). Interestingly, SEM images indicate that the cell body is subject to torsional strain, possibly generated by the flagellum. At the flagellar pocket where the flagellum emerges from the cytoplasm, there is a preferred LH chirality for the flagellum, consistent with earlier studies (24). As an independent test, we labeled the flagellum of PCF cells with a PFR2-GFP fusion protein and imaged these cells by three-dimensional (3D) confocal microscopy. In a representative 3D image (Fig. 4*C* and Movie S5), the flagellum (*green*) wraps around the surface of the cell body (*red*) and exhibits RH chirality near the base and LH chirality near the tip, forming a minus kink (*white arrows*).

Cell Body: Configurational Changes, Viscous Drag, and Torsional Stress. Arrival of kinks at the posterior end of the cell appears to correlate with transitions of the main body of the cell between two dominant configurations (see Figs. 1*B* and 2, Movies S1–S4). The configurational changes take place through alternating clockwise and counterclockwise rotations of the posterior end. In other words, the posterior end rocks back and forth about its own axis rather than completing full 360° rotations. The average frequency of the rocking motion of the posterior end was 5 ± 3 flips per second (calculated from five cells and 34 individual flips), compared to 19 ± 3 flips per second at the anterior end. The fact that the rotation frequency decreases significantly along the body of *T. brucei* is interesting. Different sections of a filament that supported a helical wave with a frequency gradient would, over time, be rotated with respect to each other over arbitrarily large angles, which for *T. brucei* would not be consistent with the mechanical integrity of the cell body. The reversals in rotation observed in *T. brucei* are thus necessary to maintain the frequency gradient.

The observation that the smaller anterior end of the body performs high-frequency complete rotations, while the larger posterior end only performs a low-frequency rocking motion, suggests a rationale why this may be an efficient mode of propagation for a microorganism with the asymmetric cell structure of *T. brucei*, given that at low Reynolds number viscous forces dominate (25). Note that a purely reciprocal motion (i.e., one that is symmetric under time reversal) cannot provide a net propulsive force to a microorganism, so the reciprocal rocking motion of the posterior end of *T. brucei* could not contribute a net propulsive force. On the other hand, the sequence of kinks traveling from the anterior to the posterior end separating helical sections with opposite chirality and opposite rotation direction obviously is nonreciprocal, and could therefore contribute a net propulsive force. Next, it follows from elementary hydrodynamics that a tapering cylindrical body rotating around its axis in a fluid is subject to a retarding viscous torque-per-unit length (τ_R) exerted by the surrounding medium that resists the rotation. This torque-per-unit length at a given point along the body is proportional to the local cross-section:

$$\tau_R = -4\pi\eta R_B^2 \omega_B \qquad [1]$$

where η is the viscosity of the surrounding medium, R_B the radius of the cross section of the cell body at that point, and ω_B the rotation rate of the body. If, for example, we model the main body of *T. brucei* as a cylinder with a length L of $\approx$20 μm and a (constant) radius of $\approx$1 μm, then the power dissipated by viscous loss in water at the 20-Hz rotation rate of the tip would be substantial: about 10^4 times the ATP hydrolysis energy per second. Reducing this rotation frequency by a factor of four—the typical frequency reduction factor between posterior and anterior ends of *T. brucei*—reduces the power dissipation by more than an order of magnitude because power is proportional to the square of the rotation frequency. For a case in which the radius of the cell body near the anterior end is about five times less than that near the posterior end, a reasonable estimate for *T. brucei*, the viscous torque-per-unit length near the anterior end is about 25 times less than that near the posterior end, thus roughly compensating for the frequency increase of the anterior end. If the flagellum produced helical waves of uniform

chirality, then the posterior and anterior ends of the cell would necessarily rotate at the same "global" rate, which would be slowed greatly by the viscous torque on the cell body near its larger posterior end. The frequency gradient thus allows for high rotation rates at the smaller anterior end, which provides the traction force that pulls the cell body along, combined with reduced rotation rates toward the larger posterior end, which reduces viscous drag. Additionally, because the flagellum is attached laterally along the length of the cell body, a helical wave of the flagellum necessarily applies a torsional stress to the cell body, as also suggested by SEM images (see Fig. 4 *A* and *B*). Depending on the degree of viscoelasticity of the cell body, the cell body may well be able to store a significant amount of torsional elastic energy in reversible deformation of the microtubule cytoskeleton. This elastic energy could then be released when the flagellum started to rotate in the opposite direction, much like the rubber motor of a toy plane.

Rapid Swings of the Flagellar Tip of BSF Cells. Despite overall similarity, there is an interesting difference between the motilities of BSF and PCF cells. The anterior end of BSF cells exhibits more frequent and more pronounced movements than that of PCF cells under similar conditions (Fig. 5 *A* and *B*). Rapid swings of BSF flagellar tips were observed following large angle bends of this portion of the flagellum (Fig. 5*C*), a feature absent from PCF cells. To quantitatively analyze the rapid swings of the flagellar tip, we extracted 12 image sequences from two BSF cells undergoing fast forward locomotion. Each of the 12 trajectories (Fig. 5*D*) represents the distance traveled by the flagellar tip in each image sequence plotted as a function of the time elapsed (a linear fit of the average trajectories is shown as a *dashed line*). The slope of each trajectory corresponds to the velocity. The highest recorded velocity of the flagellar tip is 673 μm/s, while the average velocity (i.e., the slope of the dashed line) is 510 μm/s (see the *SI Text* for details). Note that these observations could not have been made with conventional video frame rates, suggesting that millisecond DIC microscopy could be a useful tool for exploring flagellar and ciliary motility in other organisms (26–29).

BSF Motility in Infected Mouse Blood. Our studies of *T. brucei* motility so far were carried out in standard culture medium used for most studies of trypanosome motility, which has a measured viscosity close to that of water (0.95cSt). In contrast, the macroscopic viscosity of human blood is about 35 times higher than that of water. What is perhaps most relevant is that in blood, the dense distribution of erythrocytes presents to *T. brucei* a highly inhomogeneous, although deformable, labyrinth that it must negotiate. Typical sizes of the free spaces of this labyrinth can be small compared to the length of a single BSF cell. To examine *T. brucei* motility in a more native medium, we investigated BSF cells in whole blood obtained from infected mice, 3 to 5 days after infection. Millisecond DIC images of actively swimming BSF *T. brucei* in infected mouse blood revealed the same motility motifs observed with cultured parasites (Fig. 6 *A* and *B*, Movie S6). Rapid swings of the flagellar tip were particularly striking, as they can be observed initiating contact with host blood cells and deforming them significantly (Fig. 6*C*). Comparison with the measured force-deformation curves of erythrocytes (30) indicates that the flagellum is capable of exerting forces in the 300 pN range (see the *SI Text* and Table S1).

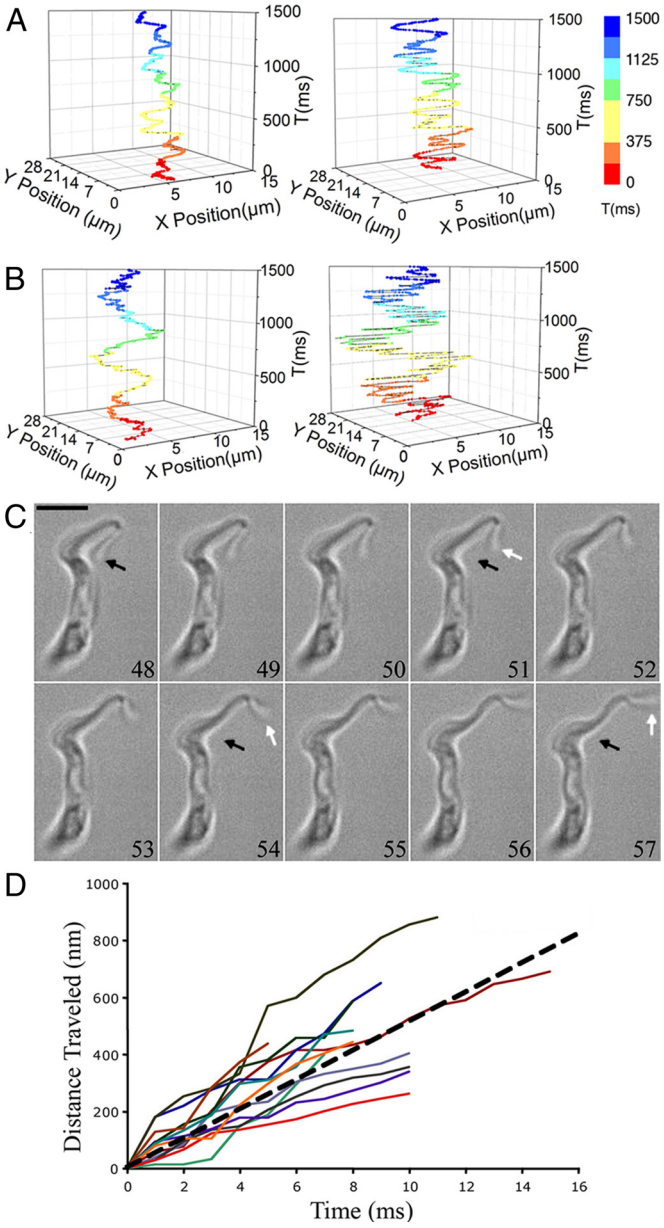

Fig. 5. Quantification of the motility of *T. brucei* cells. (*A*) Trajectory of the anterior (*Right*) and posterior (*Left*) end of a PCF cell as a function of time, where each color represents a different time period. (*B*) Trajectory of the motion of the anterior (*Right*) and posterior (*Left*) end of a BSF cell as a function of time. (*C*) Rapid motion of the BSF flagellar tip with a speed of 673 μm/s. White arrows show motion of the flagellar tip and the black arrows point to the initial tip position. The numerical numbers are in millisecond. (Scale bar, 5 μm.) (*D*) Twelve trajectories of rapid swings of the flagellar tip from two BSF cells of which the slopes represent the velocities of the flagellar tip swings. The average velocity (i.e., the slope of the dashed line) is 510 μm/s.

Discussion

Using millisecond DIC microscopy, supplemented by SEM and 3D confocal microscopy, we have found that forward *T. brucei* motility is characterized by (*i*) tip-to-base propagation of kinks separating LH and RH helical waves, (*ii*) very high motility of the flagellum tip in BSF cells, and (*iii*) a pronounced rotation-frequency gradient along the cell body, with the anterior end performing rapid full rotations while the posterior end rocks back and forth more slowly. This specialized form of motility appears to reduce viscous dissipation by minimizing rotary motion of the large posterior end of the cell, while allowing *T. brucei* to negotiate complex viscous environments, such as mammalian blood.

As noted earlier, the closest resemblance between the motility of *T. brucei* and that of other microorganisms is the prokaryote *Spiroplasma* (21, 31, 32). A comparison between these two widely divergent organisms is instructive. Both move in a zig-zag pattern, as kinks between waves of opposite chirality travel from the anterior to the posterior end. One can apply the theoretical analysis of kink motion in *Spiroplasma* (22) to *T. brucei* to argue that, also for *T.*

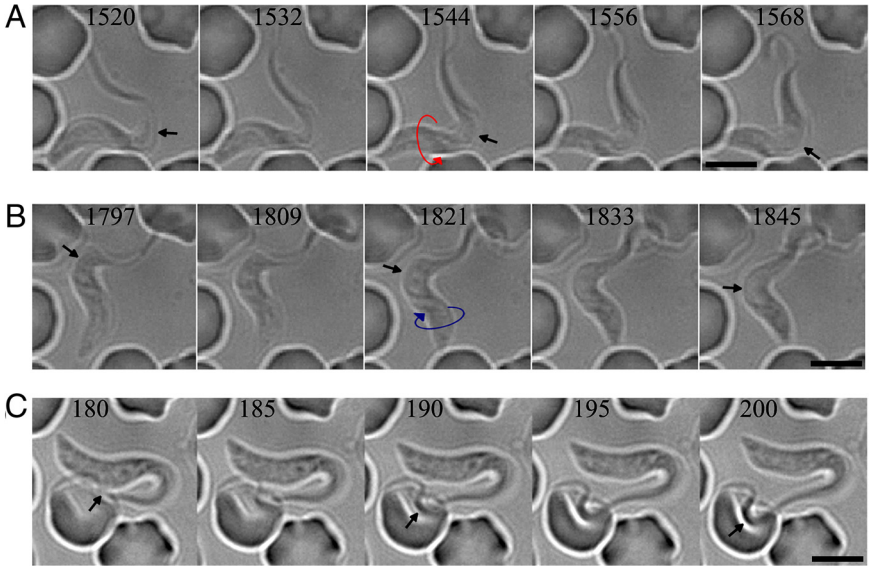

Fig. 6. Millisecond DIC microscopy imaging and analysis of BSF cell motility in infected mouse blood. (*A*) Image sequence of a BSF cell exhibiting bihelical waves separated by a plus kink, where the posterior end rotates clockwise, as indicated by the visible flagellum. The arrows pointing to the center of the kink show the kink propagation from the flagellar tip to base. The numerical values are in milliseconds. (Scale bars, 5 μm.) (*B*) Image sequence of the same BSF cell showing a minus kink where the posterior end rotates counterclockwise. (*C*) Rapid swing of the flagellum tip of the BSF cell was observed initiating contact with a host red blood cell over a time period of 20 ms.

brucei, the propulsive mechanism should be recoil against the motion of fluid carried backwards by the traveling kinks. However, whereas in *Spiroplasma* there is a preferred timing difference between kinks, which is consistent with the theoretical analysis, we encountered a broad distribution of timing differences, ranging between 150 and 300 ms. In addition, typical kink velocities of *T. brucei* (see Fig. 3*B*) are about an order of magnitude larger than that of *Spiroplasma* (about 10 μm/s), which may be because of the fact that *T. brucei* can recruit the efforts of large numbers of dynein molecular motors distributed along the axoneme (see below), whereas *Spiroplasma* presumably can rely on only a few motors. Interestingly, despite the higher kink velocity in *T. brucei*, the center of mass velocities of the two organisms is similar (in the range of 10 μm/s). This presumably reflects the larger viscous dissipative losses and also the larger mass of *T. brucei*, which by momentum conservation reduces the forward recoil velocity against the backward movement of fluid carried by the kinks. A key difference between *T. brucei* and *Spiroplasma* morphology is that *T. brucei* has a pronounced gradient in its body plan, while the body plan of *Spiroplasma* is so well described by a uniform helix (in the absence of kinks) that it is difficult to distinguish the anterior and posterior ends. In terms of motility, this translates into a uniform rotation frequency for *Spiroplasma* but a pronounced frequency gradient for *T. brucei*.

The eukaryotic axoneme is one of the most conserved structures in biology and was likely present in the last common ancestor of all extant eukaryotes (33). Axoneme motility is mediated by thousands of dynein motors that drive sliding and, ultimately, bending of microtubule doublets in the axoneme (34, 35). The switch point hypothesis is a generally accepted paradigm for wave propagation along the axoneme (36, 37). At its most basic, this hypothesis posits that axonemal dyneins are divided into two opposing groups, on either side of the axoneme, and that these groups are alternately activated or inactivated to cause axoneme bending in one direction or the other, thereby producing a plane wave. It has been demonstrated theoretically that arrays of coupled motor proteins subject to an external load can indeed switch collectively between two alternate directions of motion (38). Similarly, helical waves could be generated by assuming that the dynein motors also apply a rotary twist on each pair of microtubules of either chirality, thereby imposing a net twist on the cylindrical array of all nine outer doublet microtubules that would turn the plane wave into a helical wave, as has been proposed for waves in cilia (39). In such a model, the frequency of rotation would not be fixed but determined by the local, external load on the flagellum, determined in turn by the local radius of the flagellum. Because either helicity would be possible, there would now be dynamic instead of structural stability. Collective switching between these two helicity states, similar to the switch-point hypothesis, could then produce an array of moving kinks.

In summary, through quantitative and theoretical analysis of *T. brucei* motility, our results offer insights for considering propulsive mechanisms of microorganisms and provide new detail on an important, yet poorly understood, feature of trypanosome biology.

Materials and Methods

Millisecond DIC microscopy. A light microscope with DIC optics was assembled as follows. A Nikon Eclipse TE 2000-U inverted microscope was equipped with a Nikon Plan Apochromat 100× infinity-corrected oil DIC objective, which has a numerical aperture of 1.40 and a working distance of 0.13 mm. An open air motility chamber was placed on the microscope consisting of a glass slide, separated from a cover glass by an ≈200-μm spacer (40), placed onto the objective immersion oil. Cells were placed into the chamber in a volume of ≈100 μl in log phase. Illumination of the cells was achieved by using a Nikon 100W mercury lamp powered by an 18V to 40V source (Chiu Technical Instruments). Images were acquired using a latest generation CMOS-based Photron SA1.1 camera (Photron USA, Inc.) with 8-Gb onboard memory and a millisecond timescale.

Trypanosome Cell Maintenance and Motility Assays. PCF 29–13 and BSF-SM cells (41) were used throughout these experiments and maintained as previously described (9, 42). a Z1 Coulter Particle Counter (Beckman Coulter) to monitor cell doubling. For motility assays, cells were taken from mid-logarithmic phase cultures and placed in poly(L-glutamate)-treated glass motility chambers, described above, then imaged by using the millisecond DIC microscope. PCF cells were assayed at 25 °C, while BSF cells were assayed at 37 °C. Cells were not assayed for more than 15 min, and analyses were restricted to forward migrating cells. Image sequence acquisition, analysis, and quantification were performed as described in the *SI Text*.

Generation of GFP-PFR2 Cell Lines. The ORF of PFR2 (GenDB ID Tb927.8.4970) was PCR amplified from genomic DNA using Platinum Pfx polymerase (Invitrogen) according to the manufacturer's instructions. The forward and reverse primers used were as follows: PFR2-f 5′-TCTAGAATGAGCGGAAAGGAAGTTGAA-3′, forward. PFR2-r 5′-GGATCCCTACTGAGTGATCTGCGGC-3′, reverse (underlined are the 5′ XbaI and BamHI sites). The PCR product was ligated into a Zero Blunt TOPO PCR Cloning Kit vector (Invitrogen). The internal NotI site of the *PFR2* gene was destroyed by site-directed mutagenesis (changing C1773 into G) using a QuikChange Site-directed Mutagenesis Kit (Stratagene). The sequence was verified by sequencing at the University of California at Los Angeles genomics center. The gene encoding the PFR2 protein was subcloned using XbaI and BamHI sites into pKH10 (40, 41, 43). The construct was linearized using NotI, ethanol precipitated and transfected into PCF 29–13 cell line, as previously described (10, 42).

Transfectants were selected with 2.5 μg/ml Phleomycine (Cayla) and clonal lines were obtained by limited dilution. Individual clones were analyzed for the expression of the GFP-PFR2 fusion protein 48 h after induction with 1 μg/ml tetracycline.

Fluorescent Labeling and Confocal Microscopy Imaging of GFP-PFR2 Cells. For 3D confocal microscopy, cells expressing GFP-PFR2 (described above) were induced for 48 h with 1 μg/ml tetracycline, then washed once in prewarmed PBS and labeled with 0.5 μM CellTracker red, CMTPX (Molecular Probes, Invitrogen), in PBS for 15 min at 27 °C. Labeled cells were washed three times in prewarmed culture media. Cells were recovered for 5 min in culture media and fixed by adding paraformaldehyde (in PBS) to final concentration of 4% for 15 min directly in the labeled culture (23). Fixed cells were adhered to polyL-Lysine coated slides for 20 min. Slides were washed once with PBS, blocked in PBS containing 0.1-mM glycine for 10 min, and mounted with Vectashield mounting medium (Vector Laboratories). Slides were then imaged using a Leica TCS-SP2-AOBS Multiphoton-FLIM confocal microscope using a 63× oil immersion objective. Images were acquired using the Leica confocal software supplied with the microscope. For 3D reconstruction of fixed cells, a series of images was acquired for the red (605 nm) and green (535 nm) emission channels in 0.35-μm increments for a distance of 12.2 μm. Processing and 3D rendering of images were carried out using the National Institutes of Health ImageJ software.

Millisecond DIC Imaging of BSF *T. brucei* in Infected Mouse Blood. Bloodstream form single marker cells were maintained in vitro as previously described (9). BALB/c mice (Jackson Laboratories) were inoculated with 100 mid-log phase cells intraperitonealy in warm sterile PBS pH 7.35 (Gibco) containing 1% glucose (44). Blood samples, 3 to 5 days after infection, were collected in heparinized capillary tubes (Fisher Scientific), monitored for parasitemia by counting in a hemocytometer, and imaged by the millisecond DIC microscope.

SEM Imaging of Rapid-Fixed PCF and BSF Cells. We adopted a rapid-fixation technique optimized to preserve flagellar waveforms (23). Cells were harvested by centrifugation, resuspended in fresh medium, recovered for 30 min, and then fixed by adding paraformaldehyde/glutaraldehyde to final concentration of 3% directly in the culture medium, fixed for 5 min, diluted to 1% fixative with 0.2M sodium cacodylate buffer (pH 7.4), and allowed to settle onto cover slips for 1 h. Fixative was removed and samples were dehydrated in ethanol. Samples were then dried overnight, sputter-coated with gold and imaged using a JEOL JSM-6700F FESEM.

Further details about image acquisition and analysis, measurements of cell and kink velocity, and determination of flagellum tip motion are provided in the *SI Text*.

ACKNOWLEDGMENTS. We thank W. Shi, C. J. Brokaw, and L. Simpson for constructive comments, H. Jiang for assistance with the SEM images, as well as L. Bentolila and M. Schibler of the advanced light microscopy facility at the California NanoSystems Institute. This work was supported in part by the National Science Foundation (Grant DMR-0520894), National Institutes of Health/National Institute of Allergy and Infectious Diseases (Grant AI052348), the Alfred P. Sloan foundation, the Howard Hughes Medical Institute Gilliam fellowship for advanced studies, the Ruth L. Kirschstein National Research Service Award (GM07185), the Burroughs Wellcome Fund, and a University of California at Los Angeles Molecular Biology Interdepartmental Whitcome fellowship.

1. Legros D, et al. (2002) Treatment of human African trypanosomiasis—present situation and needs for research and development. *Lancet Infect Dis* 2:437–440.
2. Welburn SC, Odiit M (2002) Recent developments in human African trypanosomiasis. *Curr Opin Infect Dis* 15:477–484.
3. Van Den Abbeele J, Claes Y, van Bockstaele D, Le Ray D, Coosemans M (1999) *Trypanosoma brucei* spp. development in the tsetse fly: Characterization of the post-mesocyclic stages in the foregut and proboscis. *Parasitology* 118(Pt 5):469–478.
4. Vickerman K, Tetley L, Hendry KA, Turner CM (1988) Biology of African trypanosomes in the tsetse fly. *Biol Cell* 64:109–119.
5. Pepin J, Donelson JE (1999) *African Trypanosomiasis (Sleeping Sickness), in Tropical Infectious Diseases: Principles, Pathogens and Practice*. Guerrant R, Walker DH, Weller PF, Editors. (Churchill Livingstone: Philadelphia, PA).
6. Mulenga C, Mhlanga JD, Kristensson K, Robertson B (2001) *Trypanosoma brucei brucei* crosses the blood-brain barrier while tight junction proteins are preserved in a rat chronic disease model. *Neuropathol Appl Neurobiol* 27:77–85.
7. Engstler M, et al. (2007) Hydrodynamic flow-mediated protein sorting on the cell surface of trypanosomes. *Cell* 131:505–515.
8. Broadhead R, et al. (2006) Flagellar motility is required for the viability of the bloodstream trypanosome. *Nature* 440:224–227.
9. Ralston KS, Hill KL (2006) Trypanin, a component of the flagellar dynein regulatory complex, is essential in bloodstream form African trypanosomes. *PLoS Pathog* 2:e101.
10. Ralston KS, Lerner AG, Diener DR, Hill KL (2006) Flagellar motility contributes to cytokinesis in *Trypanosoma brucei* and is modulated by an evolutionarily conserved dynein regulatory system. *Eukaryot Cell* 5:696–711.
11. Kohl L, Robinson D, Bastin P (2003) Novel roles for the flagellum in cell morphogenesis and cytokinesis of trypanosomes. *EMBO J* 22:5336–5346.
12. Moreira-Leite FF, Sherwin T, Kohl L, Gull K (2001) A trypanosome structure involved in transmitting cytoplasmic information during cell division. *Science* 294:610–612.
13. Bastin P, Sherwin T, Gull K (1998) Paraflagellar rod is vital for trypanosome motility. *Nature* 391:548.
14. Ginger ML, Portman N, McKean PG (2008) Swimming with protists: Perception, motility and flagellum assembly. *Nat Rev Microbiol* 6:838–850.
15. Hill KL (2003) Biology and mechanism of trypanosome cell motility. *Eukaryot Cell* 2:200–208.
16. Kohl L, Bastin P (2005) The flagellum of trypanosomes. *Int Rev Cytol* 244:227–285.
17. Walker PJ (1961) Organization of function in trypanosome flagella. *Nature* 189:1017–1018.
18. Gruby M (1843) Analysis and observation of a novel hematozoan species, *Trypanosoma sanguinis*. *C R Hebd Seqnces Acad Sci* 17:1134–1136.
19. Turner L, Ryu WS, Berg HC (2000) Real-time imaging of fluorescent flagellar filaments. *J Bacteriol* 182:2793–2801.
20. Darnton NC, Turner L, Rojevsky S, Berg HC (2007) On torque and tumbling in swimming *Escherichia coli*. *J Bacteriol* 189:1756–1764.
21. Shaevitz JW, Lee JY, Fletcher DA (2005) Spiroplasma swim by a processive change in body helicity. *Cell* 122:941–945.
22. Yang J, Wolgemuth CW, Huber G (2009) Kinematics of the swimming of spiroplasma. *Phys Rev Lett* 102:218102.
23. Mitchell DR (2003) Orientation of the central pair complex during flagellar bend formation in *Chlamydomonas*. *Cell Motil Cytoskeleton* 56:120–129.
24. Ralston KS, Hill KL (2008) The flagellum of *Trypanosoma brucei*: New tricks from an old dog. *Int J Parasitol* 38:869–884.
25. Purcell EM (1977) Life at low Reynolds number. *Am J Phys* 45:3–11.
26. Bray D (2001) *Cell Movements: From Molecules to Motility* (Garland Pub., New York) 2nd Ed pp. xiv, 372.
27. Satir P, Christensen ST (2007) Overview of structure and function of mammalian cilia. *Annu Rev Physiol* 69:377–400.
28. Brokaw CJ (2008) Thinking about flagellar oscillation. *Cell Motil Cytoskeleton* 66:425–436.
29. Berg HC (2003) The rotary motor of bacterial flagella. *Annu Rev Biochem* 72:19–54.
30. Heinrich V, Ounkomol C (2007) Force versus axial deflection of pipette-aspirated closed membranes. *Biophys J* 93:363–372.
31. Wada H, Netz RR (2007) Model for self-propulsive helical filaments: Kink-pair propagation. *Phys Rev Lett* 99:108102.
32. Gilad R, Porat A, Trachtenberg S (2003) Motility modes of Spiroplasma melliferum BC3: A helical, wall-less bacterium driven by a linear motor. *Mol Microbiol* 47:657–669.
33. Mitchell DR (2007) The evolution of eukaryotic cilia and flagella as motile and sensory organelles. *Adv Exp Med Biol* 607:130–140.
34. Lindemann CB (2007) The geometric clutch as a working hypothesis for future research on cilia and flagella. *Ann N Y Acad Sci* 1101:477–493.
35. Hines M, Blum JJ (1983) Three-dimensional mechanics of eukaryotic flagella. *Biophys J* 41:67–79.
36. Satir P, Sale WS (1977) Tails of tetrahymena. *J Protozool* 24:498–501.
37. Satir P, Matsuoka T (1989) Splitting the ciliary axoneme: Implications for a ''switch-point'' model of dynein arm activity in ciliary motion. *Cell Motil Cytoskeleton* 14:345–358.
38. Badoual M, Julicher F, Prost J (2002) Bidirectional cooperative motion of molecular motors. *Proc Natl Acad Sci USA* 99:6696–6701.
39. Hilfinger A, Julicher F (2008) The chirality of ciliary beats. *Phys Biol* 5:16003–16015.
40. Baron DM, Ralston KS, Kabututu ZP, Hill KL (2007) Functional genomics in *Trypanosoma brucei* identifies evolutionarily conserved components of motile flagella. *J Cell Sci* 120:478–491.
41. Wirtz E, Leal S, Ochatt C, Cross GA (1999) A tightly regulated inducible expression system for conditional gene knock-outs and dominant-negative genetics in *Trypanosoma brucei*. *Mol Biochem Parasitol* 99:89–101.
42. Hutchings NR, Donelson JE, Hill KL (2002) Trypanin is a cytoskeletal linker protein and is required for cell motility in African trypanosomes. *J Cell Biol* 156:867–877.
43. Hill KL, Hutchings NR, Grandgenett PM, Donelson JE (2000) T lymphocyte-triggering factor of African trypanosomes is associated with the flagellar fraction of the cytoskeleton and represents a new family of proteins that are present in several divergent eukaryotes. *J Biol Chem* 275:39369–39378.
44. Lumsden WH, Herbert WJ (1975) Pedigrees of the Edinburgh trypanosoma (Trypanozoon) antigenic types (ETat). *Trans R Soc Trop Med Hyg* 69:205–208.